

Interactive Force-Impedance Control

Fan Shao¹, Satoshi Endo², Sandra Hirche², Fanny Ficuciello¹

Abstract— Human collaboration with robots requires flexible role adaptation, enabling robot to switch between active leader and passive follower. Effective role switching depends on accurately estimating human intention, which is typically achieved through external force analysis, nominal robot dynamics, or data-driven approaches. However, these methods are primarily effective in contact-sparse environments. When robots under hybrid or unified force-impedance control physically interact with active humans or non-passive environments, the robotic system may lose passivity and thus compromise safety. To address this challenge, this paper proposes the unified Interactive Force-Impedance Control (IFIC) framework that adapts to the interaction power flow, ensuring effortless and safe interaction in contact-rich environments. The proposed control architecture is formulated within a port-Hamiltonian framework, incorporating both interaction and task control ports, through which system passivity is guaranteed.

I. INTRODUCTION

With the development of lightweight collaborative robots, physical human-robot interaction (pHRI) provides operators a direct and intuitive ways to manipulate robots according to their intentions. Research in this field has primarily focused on human safety, physical fatigue, and intention estimation. Among pHRI tasks, trajectory tracking and regulation (i.e., compliance control with a stationary desired pose) are the most widely studied, while relatively fewer studies have addressed direct force control. In trajectory tracking or regulation tasks, where contact primarily arises from the human, signals such as external wrenches, joint torque, and robot dynamics can effectively convey human intentions to the robot. Human intention estimation methods include external force analysis in the time or frequency domain [1] [2], nominal robot dynamics, and data-driven approaches such as model-free neural network, model-based human impedance models, Gaussian process regression [3], and machine learning techniques. Some approaches assume consistent human-guidance forces during cooperation [4], while others exploit the derivative of force frequency components for rapid distinction between cooperative forces and collisions [5]. Deviations from nominal robot dynamics can also indicate human interaction through arm stiffening [6]. Bayesian neural networks combined with human model learning can improve intention estimation accuracy and reduce human–robot disagreement [7]. Machine learning applied to joint torque sensing has enabled intrinsic tactile

perception [8], while multimodal intention recognition integrating vision and tactile data outperforms monomodal methods [9]. Nevertheless, these methods are generally valid only in contact-sparse environments. To address the challenges of passivity and safety in contact-rich pHRI, energy tank based methods have been proposed. A virtual energy tank supplies energy to the controller [10], regulates impedance parameter adaptation, and attenuates control output when needed. By defining an appropriate energy budget, the tank stores dissipated energy and compensates for non-passive behaviors that increase system energy, such as variations in inertia or stiffness in impedance/admittance control [11] [12]. Energy tanks have also been used in teleoperated robotic surgery to ensure passivity during stiffness adaptation and mode switching between autonomous and teleoperated control [13]. Furthermore, the tank energy has been utilized as an indicator of human interaction intent [4], allowing the robot to either track predefined trajectories or adapt compliantly to human input.

For tasks requiring direct force control, such as polishing [14] and grinding [15], hybrid force-impedance control (HFIC) is typically employed. In HFIC, the controller enforces accurate force control in the constrained space (C-Space) and compliant behavior in the unconstrained space (U-Space), where orthogonality between motion and force subspaces is ensured through a selection matrix. However, when the environment model is uncertain or unavailable, this orthogonality breaks down, potentially leading to passivity violations. To mitigate this, Haddadin, Schindlbeck *et.al* introduced the Unified Force-Impedance Control (UFIC) [16] [17], which employs separate virtual energy tanks for the force and impedance controllers to maintain system passivity. Although UFIC effectively addresses controller-induced non-passive behaviors such as contact loss in force control, it assumes a passive environment and thus faces challenges when dealing with non-passive interactions induced by either the human or the environment. In contact-rich environments, both humans and the environment can inject interaction power into the system. For instance, soft contacts in the C-Space or frictional and clamping effects in the U-Space may produce environmental power flows that resemble human intent. Misclassification of such signals can compromise both safety and responsiveness. Existing solutions either rely on a priori environment models or employ complex external sensors. For example, in structured environments, the force controller may be simply switched off when the end-effector (EE) leaves the contact surface due to human guidance [18], while in multimodal sensing, which combines force/torque (F/T) and electromyography (EMG) signals [19] or tactile

¹ PRISMA Lab, Electrical Engineering and Information Technology Department, University of Naples Federico II, Naples, Italy
fan.shao@unina.it, fanny.ficuciello@unina.it

² Chair of Information-oriented Control (ITR), Electrical and Computer Engineering Department, Technical University of Munich, Munich, Germany s.endo@tum.de, hirc@cit.tum.de

skins [20], can improve human environment differentiation at the cost of increased hardware complexity.

Passivity-based control, originally proposed in [21], models robotic systems through port-based energy exchange, where the environment and robot interact via conjugate effort-flow pairs, e.g., $(\dot{x}, -F_{ext})$ and (\dot{x}, F_{ext}) . Building upon this concept, UFIC ensures passivity with respect to the controller's internal power flows. However, the non-passive interaction power $\dot{x}^T F_{ext}$ generated by human or environmental interactions can still inject energy into the system.

To overcome this limitation, this paper proposes a passivity-guaranteed IFIC. By explicitly extracting the interaction port from the controller, virtual energy tanks are connected to both the interaction and control ports via their input-output pairs to capture and regulate the corresponding power flows. The controller output is then adaptively adjusted according to the detected non-passive interaction or control behavior. This mechanism ensures system passivity while preserving task performance and safe full-body interaction. Thanks to the power-flow-valve-controlled energy tank design, the proposed method achieves safe, responsive, and intuitive pHRI in contact-rich scenarios. The remainder of this paper is organized as follows. Section II presents the calculation of interaction power and the design of system ports. Section III details the design of the IFIC framework. Section IV verifies the passivity of the proposed system. Section V describes the experimental validation, and Section VI concludes the paper.

II. INTERACTION POWER PAIR AND PORT DESIGN

A. Interaction Power

The classification of force-impedance control tasks can be based on the kinematic constraints imposed by contact surfaces [22]. For instance, in an unconstrained 2D surface polishing task, the desired Cartesian velocity and wrench are defined as $\dot{x}_d = [(v_{d,x} \ v_{d,y} \ 0), (0 \ 0 \ \omega_{d,z})]^T$ and $F_d = [(0 \ 0 \ f_{d,z}), (\tau_{d,x} \ \tau_{d,y} \ 0)]^T$, respectively. In this task configuration, $\dot{x}_d^T F_d = 0$. The reaction wrench exerted by the environment arises from motion-induced friction and force control interactions: $F_r = [(f_{r,x} \ f_{r,y} \ -f_{d,z}), (-m_{d,x} \ -m_{d,y} \ \tau_{r,z})]^T$.

Environmental or human interactions can occur in either the force or impedance control spaces. In most force control tasks, the force control frame aligns with the EE frame. Let ${}^W\mathbf{R}_{\mathcal{F}} \in \mathbb{R}^{3 \times 3}$ denote the rotation matrix representing the orientation of the force control frame \mathcal{F} with respect to the world frame \mathcal{W} . Then, $F_d = {}^W\mathbf{R}_{\mathcal{F}} F_d^{\mathcal{F}}$, where $F_d^{\mathcal{F}} \in \mathbb{R}^6$ is the desired wrench applied by the robot to the environment, expressed in the force frame \mathcal{F} . By converting the non-zero elements of $F_d^{\mathcal{F}}$ to 1, we obtain the binary vector F_d^{bin} . The force control directional matrix in the world frame is defined as

$$\mathbf{D}_w \in \mathbb{R}^{6 \times 6} = [\underbrace{\mathbf{d}_{f,x} \mathbf{d}_{f,y} \mathbf{d}_{f,z}}_{\text{force}} \ \underbrace{\mathbf{d}_{m,x} \mathbf{d}_{m,y} \mathbf{d}_{m,z}}_{\text{moment}}] \text{diag}(F_d^{bin}) \quad (1)$$

where $\mathbf{d}_{f,i} = \begin{bmatrix} {}^W\mathbf{R}_{\mathcal{F}}(:, i) \\ \mathbf{0}_{3 \times 1} \end{bmatrix} \in \mathbb{R}^6$, $\mathbf{d}_{m,j} = \begin{bmatrix} \mathbf{0}_{3 \times 1} \\ {}^W\mathbf{R}_{\mathcal{F}}(:, j) \end{bmatrix} \in \mathbb{R}^6$, and $\text{diag}(F_d^{bin})$ is the diagonal matrix. Let $\text{rank}(\mathbf{D}_w) = l$ denote the number of non-zero elements in F_d^{bin} , $0 \leq l \leq 6$. The C-Space projection matrix is defined as the span of \mathbf{D}_w 's column space: $[\mathbf{D}_w] \in \mathbb{R}^{6 \times 6} = \mathbf{D}(\mathbf{D}^T \mathbf{D})^+ \mathbf{D}^T$. The interaction power in the C-Space is given by $P_c = \dot{x}^T [\mathbf{D}_w] F_{ext}$, while the interaction power in the U-Space is calculated using the kernel of the force control directions to remove force control contributions: $P_u = \dot{x}^T \langle \mathbf{D}_w \rangle F_{ext}$, where $\langle \mathbf{D}_w \rangle = \mathbf{I} - [\mathbf{D}_w]$, and $\mathbf{I} \in \mathbb{R}^{6 \times 6}$ is identity matrix.

B. Port Allocation of Force and Impedance Control

The inverse dynamic model of an n -DOF manipulator with revolute joints can be expressed as

$$M(q)\ddot{q} + C(q, \dot{q})\dot{q} + g(q) = \tau + J^T(q)F_{ext}, \quad (2)$$

where $M(q) \in \mathbb{R}^{n \times n}$, $C(q, \dot{q}) \in \mathbb{R}^{n \times n}$, $g(q) \in \mathbb{R}^n$ are the inertia, Coriolis/centrifugal, and gravity terms, respectively; $\tau \in \mathbb{R}^n$ is the joint torque; $F_{ext} \in \mathbb{R}^6$ is the external wrench that the environment applies to the robot; $J(q) \in \mathbb{R}^{6 \times n}$ is the manipulator Jacobian; and $q, \dot{q}, \ddot{q} \in \mathbb{R}^n$ denote joint positions, velocities, and accelerations. Cartesian force control is realized as $\tau_f = J^T F_f$, with

$$F_f = K_p(F_{ext} + F_d') + F_f^{i,d}, \quad (3)$$

where

$$F_d' = {}^W\mathbf{R}_{\mathcal{F}} (F_d^{\mathcal{F}} + (F_d^{bin} - \mathbf{1}_6) \odot F_{ext}^{\mathcal{F}}), \quad (4)$$

$$F_f^{i,d} = K_i \int_0^t (F_d'(\theta) + F_{ext}(\theta)) d\theta + K_d(\dot{F}_d' + \dot{F}_{ext}) + F_d. \quad (5)$$

Here, $\mathbf{1}_6$ is the unit vector, \odot denotes the element-wise (Hadamard) product, and $K_p, K_i, K_d \in \mathbb{R}^{6 \times 6}$ are gain matrices. Gains in world frame are related to force-frame gains by

$$K_g = \begin{bmatrix} {}^W\mathbf{R}_{\mathcal{F}} & \mathbf{0}_{3 \times 3} \\ \mathbf{0}_{3 \times 3} & {}^W\mathbf{R}_{\mathcal{F}} \end{bmatrix} K_g^{\mathcal{F}} \begin{bmatrix} {}^W\mathbf{R}_{\mathcal{F}} & \mathbf{0}_{3 \times 3} \\ \mathbf{0}_{3 \times 3} & {}^W\mathbf{R}_{\mathcal{F}} \end{bmatrix}^T, \quad (6)$$

$$g \in \{p, i, d\}.$$

where $K_p^{\mathcal{F}}, K_i^{\mathcal{F}}, K_d^{\mathcal{F}}$ are diagonal matrix with nonzero diagonal entries. Considering the robot dynamics in Cartesian space:

$$\Lambda(q)\ddot{x} + \mu(q, \dot{q})\dot{x} + F_g(q) = J^{\dagger T} \tau_u + F_{ext}, \quad (7)$$

where $\Lambda(q), \mu(q, \dot{q}), F_g(q)$ are, respectively, the inertia, the Coriolis/centrifugal, and gravity in Cartesian space, and J^{\dagger} is the Moore-Penrose pseudoinverse [23]. Impedance control law in the world frame is:

$$\tau_i = J^T(\Lambda \ddot{x}_d - D_d \dot{\tilde{x}} - K_s \tilde{x} + \mu \dot{x}_d + F_g), \quad (8)$$

with $\tilde{x}(t) = x(t) - x_d(t)$, $x_d \in \mathbb{R}^6$ is the desired Cartesian pose, and $D_d \in \mathbb{R}^{6 \times 6}$, $K_s \in \mathbb{R}^{6 \times 6}$ being desired damping and stiffness matrices. The combined force-impedance control torque is $\tau_u = \tau_f + \tau_i$, leading to

$$\Lambda \ddot{\tilde{x}} + \mu \dot{\tilde{x}} + D_d \dot{\tilde{x}} + K_s \tilde{x} - F_f - F_{ext} = 0. \quad (9)$$

The system state is defined as $\tilde{p} = \Lambda \dot{\tilde{x}}$, with storage function

$$V_{i,f}(\dot{\tilde{x}}, \tilde{x}) = \frac{1}{2} \tilde{p}^T \Lambda^{-1} \tilde{p} + \frac{1}{2} \tilde{x}^T K_s \tilde{x}. \quad (10)$$

The corresponding port-based representation of (9) is

$$\begin{cases} \begin{bmatrix} \dot{\tilde{x}} \\ \dot{\tilde{p}} \end{bmatrix} = \begin{bmatrix} \mathbf{0} & \mathbf{I} \\ -\mathbf{I} & \mu + D_d \end{bmatrix} \begin{bmatrix} \frac{\partial V}{\partial \tilde{x}} \\ \frac{\partial V}{\partial \tilde{p}} \end{bmatrix} + \begin{bmatrix} \mathbf{0} \\ \mathbf{I} \end{bmatrix} \underbrace{(F_{ext} + F_f)}_u, \\ y = \dot{\tilde{x}}. \end{cases} \quad (11)$$

Here, $u = F_{ext} + F_f$ is the system input, and $y = \dot{\tilde{x}}$ is the output, $\mathbf{0}, \mathbf{I} \in \mathbb{R}^{6 \times 6}$. With u as the effort and y as the flow, the overall system power is

$$\begin{aligned} P &= y^T u = \dot{\tilde{x}}^T (F_{ext} + F_f) \\ &= \dot{x}^T F_{ext} - \dot{x}_d^T F_{ext} + \dot{x}^T F_f - \dot{x}_d^T F_f. \end{aligned} \quad (12)$$

The system ports include impedance control port $(-\dot{x}_d, F_{ext})$, force control port (\dot{x}, F_f) , and counteraction port $(-\dot{x}_d, F_f)$. Due to friction, contact loss, and impedance control counteract force control, the control power terms $-\dot{x}_d^T F_{ext}$, $\dot{x}^T F_f$, and $-\dot{x}_d^T F_f$ can be positive, and passivity w.r.t. (\dot{x}, F_{ext}) is not guaranteed. To solve this, UFIC connects energy tanks to controller ports. To further ensure safe pHRI under non-passive human and environmental interactions, port allocation is refined.

Note that $\langle \mathbf{D}_w \rangle + [\mathbf{D}_w] = \mathbf{I}$, the Cartesian force control law is equal to

$$F_f = K_p [\mathbf{D}_w] F_{ext} + \overbrace{(K_p [\mathbf{D}_w] F_d^i + F_f^{i,d})}^{F_f^r} + K_p \langle \mathbf{D}_w \rangle F_{ext} + K_p \langle \mathbf{D}_w \rangle F_d'. \quad (13)$$

The force control port is divided into four sub-ports:

$$\begin{aligned} &(\dot{x}, K_p [\mathbf{D}_w] F_{ext}), \quad (\dot{x}, F_f^r), \\ &(\dot{x}, K_p \langle \mathbf{D}_w \rangle F_{ext}), \quad (\dot{x}, K_p \langle \mathbf{D}_w \rangle F_d'). \end{aligned} \quad (14)$$

In this way, it is possible to separate and monitor the interaction power flow in the system. In the C-Space, $(\dot{x}, K_p [\mathbf{D}_w] F_{ext})$ may generate positive power $k_p P_c$ that violates passivity under human guidance or environmental impact. In U-Space, $(\dot{x}, K_p \langle \mathbf{D}_w \rangle F_{ext})$ injects negative power $\dot{x}^T K_p \langle \mathbf{D}_w \rangle F_{ext} = k' P_u$ due to friction, preserving passivity. However, non-passive interactions, such as human intentionally pushing or unintentionally colliding with the robot body in the U-Space, can generate positive P_u that violates passivity. To maintain passivity, the energy tank should be properly designed and connected to the controller port to ensure power consistency, ensuring no energy is generated or dissipated as power flows between the tank and the controller. Impedance control directional matrix $\mathbf{D}_i \in \mathbb{R}^{6 \times 6}$ is defined similarly to \mathbf{D}_w . The impedance control can be rewritten as

$$\begin{aligned} \tau_i &= J^T (\Lambda \ddot{x}_d - (\lambda_c D_d \langle \mathbf{D}_i \rangle \dot{x} + D_d [\mathbf{D}_i] \dot{\tilde{x}}) \\ &\quad - K_s \tilde{x} + \mu \dot{x}_d + F_g), \end{aligned} \quad (15)$$

where λ_c modulates the damping along constrained directions. Its exact definition will be provided later in (18).

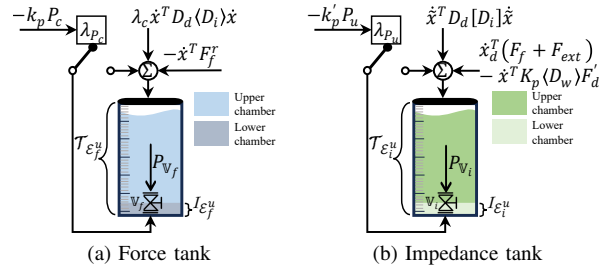


Fig. 1: Valve-controlled dual-chamber tank.

III. INTERACTIVE FORCE-IMPEDANCE CONTROL

When the controller is augmented with virtual energy tanks, each tank manages the possible passivity violations of a specific task. For example, an impedance tank addresses variable stiffness [24], and a force tank addresses force control [25]. Multiple tasks can share a single tank based on priority levels [26], with high-priority tasks are allowed more control power and may consume stored tank energy to violate passivity. In force-impedance control, the two tasks have equal priority, and pHRI may occur in either the C-Space or U-Space. Therefore, dedicated virtual energy tanks are assigned to both the force and impedance controllers.

A. Interactive Force Control

The force control tank is connected to two ports: the C-Space interaction port $(\dot{x}, K_p [\mathbf{D}_w] F_{ext})$ and the force regulation port (\dot{x}, F_f^r) . To establish a power-preserving Dirac structure linking the force tank and force controller, the corresponding force tank port is defined as $(-\dot{x}, F_f^r + K_p [\mathbf{D}_w] F_{ext})$. As shown in Fig. 1a, the force tank adopts a valve-controlled dual-chamber structure. The two chambers collectively serve the force control task, while the lower (interactive) chamber is exclusively dedicated to handling non-passive interactions. The interactive chamber connects to the $(\dot{x}, K_p [\mathbf{D}_w] F_{ext})$ port only when $P_c > 0$. Let \mathcal{E}_f and \mathcal{E}_f^i denote the total energy and the interactive chamber energy, respectively, while \mathcal{E}_f^u and \mathcal{E}_f^i represent their corresponding upper energy limits for the task and non-passive interactions.

The power flow valve \mathbb{V}_f regulates energy transfer from the upper chamber to the lower chamber at rate $P_{\mathbb{V}_f}$. When $\mathcal{E}_f = \mathcal{E}_f^u$, $P_{\mathbb{V}_f} = 0$. A small upper-energy budget $\mathcal{E}_f^u = 0.1\text{J}$ ensures that when P_c exceeds $P_{\mathbb{V}_f}$, the lower chamber energy is immediately drained. For sensitive C-Space responses to interaction, $P_{\mathbb{V}_f}$ is set to a small positive value of 0.03W , to filter out noisy F_{ext} and \dot{x} . In the absence of external interactions ($P_c < P_{\mathbb{V}_f}$), the lower interactive chamber charges according to $P_{\mathbb{V}_f} = \mathcal{E}_f^u / t_{l,f}$, where $t_{l,f}$ is the maximum loading time. A smaller $t_{l,f}$ allows faster recovery of force control post-interaction. It should be noted that the value of $P_{\mathbb{V}_f}$ should adapt to different scenarios. A smaller $P_{\mathbb{V}_f}$ increases the system's sensitivity to non-passive interactions, while a larger $P_{\mathbb{V}_f}$ helps maintain stable force regulation under disturbances.

For instance, during unintentional collisions with a human or unexpected impacts with the environment, P_{V_f} should be kept small to enhance responsiveness and safety. Conversely, when the human intentionally manipulates the object held by the robot and the force control needs to stay active, P_{V_f} should be set larger to preserve control authority. In this work, we focus on a smaller P_{V_f} configuration to evaluate the system's fast response to external interactions.

The total tank energy is defined as $\mathcal{E}_f = 1/2z_f^2$, with tank state z_f governed by:

$$(d_f, \mathcal{T}d_f, \mathcal{I})\dot{z}_f = \frac{P_f}{z_f}, \quad (16)$$

where the control power input is

$$\mathcal{P}_f = -\dot{x}^T F_f^r + \lambda_c \dot{x}^T D_d \langle \mathbf{D}_i \rangle \dot{x} - \underbrace{\dot{x}^T K_p [\mathbf{D}_w] F_{ext}}_{k_p P_c}, \quad (17)$$

and

$$\lambda_c = \begin{cases} 1, & \text{if } \mathcal{E}_f < \mathcal{E}_{f,l} + \delta_{f,h} \\ 0, & \text{else.} \end{cases} \quad (18)$$

The interactive chamber energy evolves as

$$\begin{aligned} \mathcal{E}_f(t) &= \mathcal{E}_f(t-1) + (P_{V_f} - \lambda_{P_c} k_p P_c) dt, \\ \lambda_{P_c} &= \begin{cases} 1, & \text{if } P_c > 0 \\ 0, & \text{else.} \end{cases} \end{aligned} \quad (19)$$

The damping terms $d_{f,\mathcal{T}}, d_{f,\mathcal{I}}$ are computed from the tank energy:

$$d_{f,\mathcal{S}} = \begin{cases} 1, & \text{if } \mathcal{E}_f > \mathcal{E}_{f,l} + \delta_{f,h} \\ \epsilon^{-1}, & \text{else if } \mathcal{E}_f < \mathcal{E}_{f,l} + \delta_{f,s} \\ (\cos((1 - \mathcal{A}^p) \frac{\pi}{2}) + \epsilon)^{-1}, & \text{else,} \end{cases} \quad (20)$$

with

$$\begin{aligned} \mathcal{A} &= \frac{\mathcal{E}_f - \mathcal{E}_{f,l} - \delta_{f,s}}{\delta_{f,h} - \delta_{f,s}}, \\ p &= \begin{cases} 1, & \text{if } P_c > 0 \\ 10, & \text{else.} \end{cases} \end{aligned} \quad (21)$$

Finally, the force control output is modified as:

$$F'_f = \frac{F_f}{d_{f,\mathcal{T}} d_{f,\mathcal{I}}}. \quad (22)$$

Here, $\mathcal{E}_{f,l}$ denotes the lower energy limit, while $\delta_{f,h}$ and $\delta_{f,s}$ are constant parameters satisfying $\delta_{f,h} > \delta_{f,s}$. The small constant $\epsilon = 10^{-4}$. The parameter p governs the decay rate of $d_{f,\mathcal{S}}$ with respect to the tank energy: larger p values correspond to slower decay. This design ensures that the force control becomes inactive immediately after a non-passive interaction and gradually recovers following human interaction.

B. Interactive Impedance Control

The impedance tank follows the same design as the force tank, with three ports: $(-\dot{x}, K_p \langle \mathbf{D}_w \rangle F_{ext})$, $(-\dot{x}, K_p \langle \mathbf{D}_w \rangle F'_d)$, and $(\dot{x}_d, F'_d + F_{ext})$ (Fig. 1b). Let \mathcal{E}_i and $\mathcal{I}\mathcal{E}_i$ denote the total and lower (interactive) chamber energies, respectively. \mathcal{E}_i is allocated to the impedance control task, while $\mathcal{I}\mathcal{E}_i$ handles non-passive interactions in U-Space. The upper energy limits are \mathcal{E}_i^u and $\mathcal{I}\mathcal{E}_i^u$. Due to the friction, $P_u < 0$ in the absence of external interactions. When $P_u > 0$, the interactive chamber connects to $(\dot{x}, K_p \langle \mathbf{D}_w \rangle F_{ext})$. Since $K_p \langle \mathbf{D}_w \rangle (F_{ext} + F'_d) = 0$, the connection with ports $(\dot{x}, K_p \langle \mathbf{D}_w \rangle F_{ext})$, $(\dot{x}, K_p \langle \mathbf{D}_w \rangle F'_d)$ do not affect total tank energy. The power-flow rate is set as $P_{V_i} = 0.01$ W for $P_u > 0$, and $P_{V_i} = \mathcal{E}_i^u / t_{l,i}$ for $P_u < 0$. The impedance tank dynamics are defined as

$$\begin{aligned} (d_i, \mathcal{T}d_i, \mathcal{I})\dot{z}_i &= \frac{P_i}{z_i}, \\ P_i &= \dot{x}_d^T (F'_d + F_{ext}) + \dot{x}^T D_d [\mathbf{D}_i] \dot{x} \\ &\quad - \underbrace{(\dot{x}^T K_p \langle \mathbf{D}_w \rangle F_{ext} + \dot{x}^T K_p \langle \mathbf{D}_w \rangle F'_d)}_{=0}, \end{aligned} \quad (23)$$

where z_i is the tank state, and $d_i, \mathcal{T}d_i, \mathcal{I}d_i$ are computed in the same way as for the force tank (20). The tank energy evolves as $\mathcal{E}_i = 1/2z_i^2$, and $\mathcal{E}_i(t) = \mathcal{E}_i(t-1) + (P_{V_i} - \lambda_{P_u} k'_p P_u) dt$, with $\lambda_{P_u} = 1$ if $P_u > 0$ and 0 otherwise. The desired Cartesian velocity is modified according to the damping:

$$\dot{x}'_d = \frac{\dot{x}_d}{d_i, \mathcal{T}d_i, \mathcal{I}}. \quad (24)$$

IV. PASSIVITY PRESERVING ANALYSIS

After connecting the system with the energy tanks, the overall storage function is defined as

$$V(\dot{x}, \tilde{x}, z_f, z_i) = \frac{1}{2} \tilde{p}^T \Lambda^{-1} \tilde{p} + \frac{1}{2} \tilde{x}^T K_s \tilde{x} + \frac{1}{2} z_f^2 + \frac{1}{2} z_i^2. \quad (25)$$

Let the system state and gradient of V be defined as

$$\begin{aligned} \dot{X} &:= [\dot{x}^T, \dot{\tilde{p}}^T, \dot{z}_f, \dot{z}_i]^T, \\ \nabla V &:= \left[\frac{\partial V}{\partial \dot{x}}, \frac{\partial V}{\partial \tilde{p}}, \frac{\partial V}{\partial z_f}, \frac{\partial V}{\partial z_i} \right]^T, \end{aligned} \quad (26)$$

the input vector $U \in \mathbb{R}^{18}$ is composed of three input

$$U = [u_1^T \ u_2^T \ u_3^T]^T, \quad (27)$$

with

$$\begin{aligned} u_1 &= F_{ext} + F_f, & u_2 &= -K_p [\mathbf{D}_w] F_{ext} - F_f^r, \\ u_3 &= F_f + F_{ext}. \end{aligned} \quad (28)$$

The overall system can thus be expressed as port-Hamiltonian form

$$\begin{cases} \dot{X} = \text{diag} \left(\begin{bmatrix} \mathbf{0} & \mathbf{I} \\ -\mathbf{I} & \mu + D_d \end{bmatrix}, H, G \right) \nabla V + B_{\text{tot}} U, \\ Y = [\dot{x}^T, \dot{x}^T, \dot{x}_d^T]^T, \end{cases} \quad (29)$$

where $B_{\text{tot}} \in \mathbb{R}^{14 \times 18}$

$$B_{\text{tot}} = [B_1 \ B_2 \ B_3],$$

$$B_1 = \begin{bmatrix} \mathbf{0}_{6 \times 6} \\ \mathbf{I}_{6 \times 6} \\ \mathbf{0}_{2 \times 6} \end{bmatrix}, B_2 = \begin{bmatrix} \mathbf{0}_{12 \times 6} \\ \frac{\dot{x}^T}{d_f, \tau d_f, \tau z_f} \\ \mathbf{0}_{1 \times 6} \end{bmatrix}, B_3 = \begin{bmatrix} \mathbf{0}_{13 \times 6} \\ \frac{\dot{x}_d^T}{d_i, \tau d_i, \tau z_i} \end{bmatrix}, \quad (30)$$

$$H = \frac{\lambda_c \dot{x}^T D_d \langle \mathbf{D}_i \rangle \dot{x}}{z_f^2}, \quad G = \frac{\dot{x}^T D_d [\mathbf{D}_i] \dot{x}}{z_i^2}. \quad (31)$$

The instantaneous power of the entire system becomes

$$\begin{aligned} Y^T U &= \dot{x}^T u_1 + \dot{x}^T u_2 + \dot{x}_d^T u_3 \\ &= \dot{x}^T (F_{\text{ext}} + F_f) - \dot{x}_d^T (F_{\text{ext}} + F_f) \\ &\quad - \dot{x}^T (K_p [\mathbf{D}]_w F_{\text{ext}} + F_f^r) + \dot{x}_d^T (F_{\text{ext}} + F_f) \\ &= \dot{x}^T F_{\text{ext}}, \end{aligned} \quad (32)$$

showing that energy balance is maintained and no energy is generated within the control framework. By combining (25), (9), (16) and (23), the time derivative of the system storage function can be obtained, leading to

$$\begin{aligned} \dot{V} &= \dot{x}^T F_{\text{ext}} - \dot{x}'^T D_d ([\mathbf{D}_i] + \langle \mathbf{D}_i \rangle) \dot{x}' \\ &\quad + \dot{x}^T F'_f - \dot{x}_d^T (F'_f + F_{\text{ext}}) \\ &\quad + d_{f, \tau}^{-1} d_{f, \mathcal{I}}^{-1} (-\dot{x}^T F_f^r - \dot{x}^T K_p [\mathbf{D}_w] F_{\text{ext}} + \lambda_c \dot{x}^T D_d \langle \mathbf{D}_i \rangle \dot{x}) \\ &\quad + d_{i, \tau}^{-1} d_{i, \mathcal{I}}^{-1} (\dot{x}_d^T (F'_f + F_{\text{ext}}) + \dot{x}'^T D_d [\mathbf{D}_i] \dot{x}') \\ &= \underbrace{(\lambda_c d_{f, \tau}^{-1} d_{f, \mathcal{I}}^{-1} - 1) \dot{x}^T D_d \langle \mathbf{D}_i \rangle \dot{x} + \dot{x}^T F_{\text{ext}}}_{\leq 0} \\ &\quad + \underbrace{(d_{i, \tau}^{-1} d_{i, \mathcal{I}}^{-1} - 1) \dot{x}'^T D_d [\mathbf{D}_i] \dot{x}'}_{\leq 0}. \end{aligned} \quad (33)$$

From (33), it is evident that $\dot{V} \leq \dot{x}^T F_{\text{ext}}$. Therefore, the unified IFIC maintains passivity, ensuring safe and energetically consistent interaction during human–robot collaboration.

V. EXPERIMENTS

Two pHRI scenarios were considered in our experiments: robotic table wiping and robot-assisted ultrasound scanning on a soft phantom and a human arm, as illustrated in Fig. 2. We employed a KUKA LBR Med R820 robot with 1 kHz Fast Robot Interface (FRI), configured in joint torque control mode. To achieve full-body interaction, joint torque sensors were used to calculate the external wrench F_{ext} .

In this paper, we evaluate the performance of the proposed IFIC in response to active interactions from non-passive environments. Readers are referred to the UFIC framework [17] for further details on how the task energy budget is computed to ensure task fulfillment. We compared IFIC with three approaches: UFIC, low-pass filtering (LPF) [1], and nominal dynamical system (DS) methods [27], [4]. All methods employed the same force and impedance controllers with identical parameters, including stiffness, damping, and the PID coefficients used for force control. The LPF method identifies intended contact by analyzing the force frequency and deactivates the controller upon detection. The measured

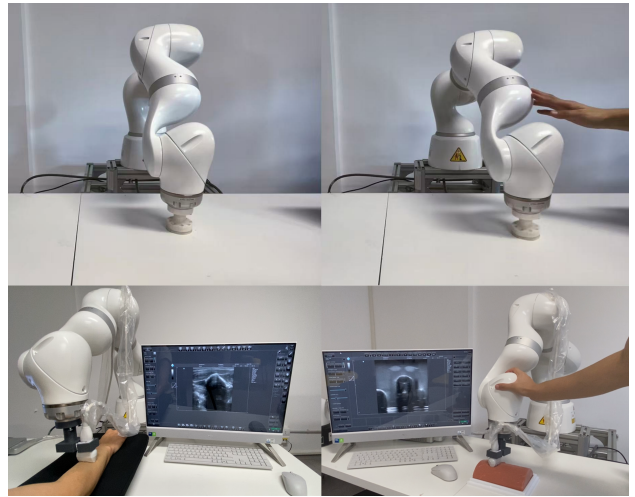


Fig. 2: Experimental setup. Top row: interactive table-wiping task. Bottom left: interactive ultrasound scanning task on human arm. Bottom right: interactive ultrasound scanning task on a soft-tissue phantom.

force signals are filtered with a bandwidth of 20 Hz to suppress noise and detect contact intent. Nominal DSs can encode different tasks. The switch between precise tracking and compliant behaviors is controlled by

$$\begin{aligned} \dot{x}_d &= (1 - h_v) \dot{x}_t + \dot{x}_a, \\ F_d &= (1 - h_f) F_t, \end{aligned} \quad (34)$$

where \dot{x}_t and F_t represent the task-specific impedance control velocity in U-Space and the desired force in C-Space generated by the robot's nominal DS, respectively, and \dot{x}_a denotes the velocity output of the admittance controller. The human-guidance ratio h_v and h_f are determined based on the stored interaction energy:

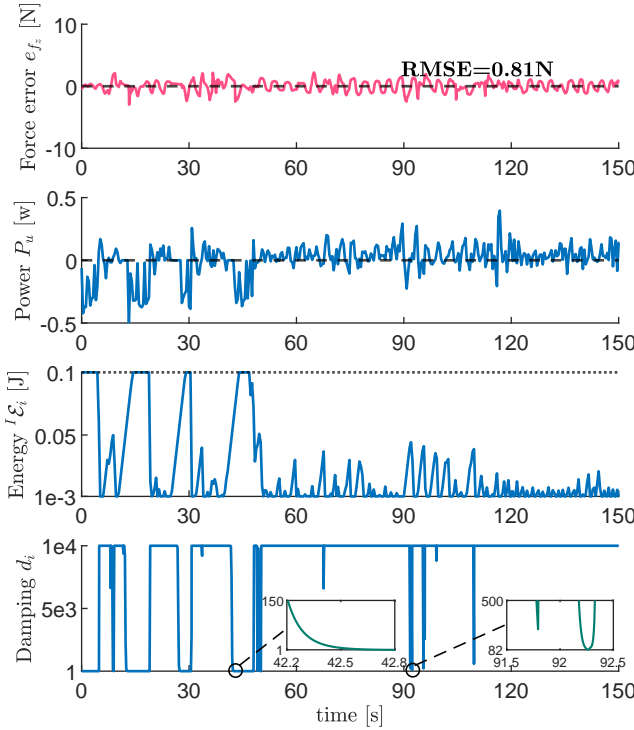
$$h = \begin{cases} 0 & \text{if } E \leq E_t \\ (E - E_t)/(E_m - E_t) & \text{else,} \end{cases} \quad (35)$$

where $E_t = 0.5$ J is the threshold that triggers the detection of human guidance.

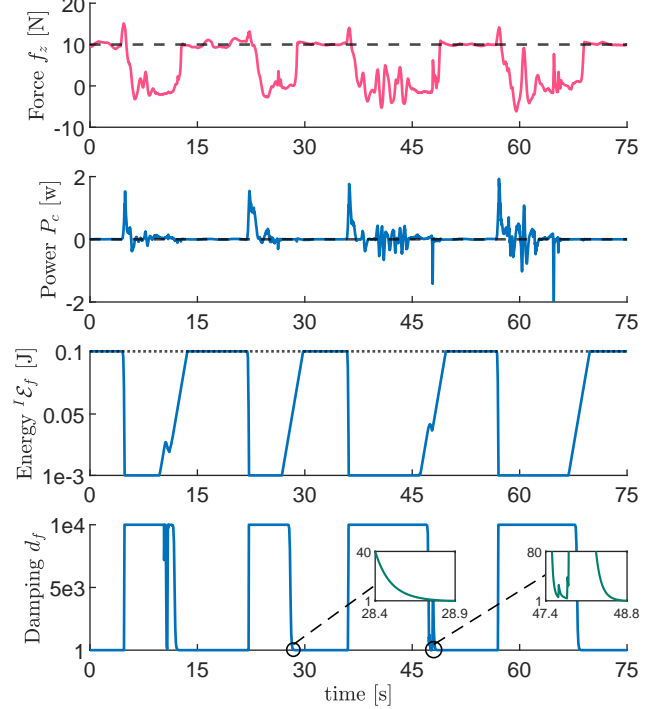
In the table wiping task, the desired contact force was set to -10N along the vertical z -direction, while the desired velocity in the xy -plane followed a sinusoidal trajectory along both x and y axes, producing a periodic reciprocating motion. For the robot-assisted ultrasound scanning task, the target force was -3 N along the z -direction. Four experiments were conducted to evaluate the performance of IFIC, and the experimental parameters are listed in TABLE I. In the first experiment, IFIC performance was assessed during the table wiping task. The second experiment compared IFIC with the alternative methods in the same task, focusing on human–robot interaction efficiency (IE) and safety. In the third and fourth experiments, robot-assisted ultrasound scanning was performed on a soft phantom and a human arm, respectively, with IFIC again compared to other approaches in terms of IE and safety.

TABLE I: Experimental parameters

	$f_{d,z}$	P_{V_f}	P_{V_i}	$\tau_{\mathcal{E}_f^u}$	$\tau_{\mathcal{E}_i^u}$	$\tau_{\mathcal{E}_f^u}$	$\tau_{\mathcal{E}_i^u}$	$t_{l,f}$	$t_{l,i}$	$K_p^{\mathcal{F}}$	$K_i^{\mathcal{F}}$	$K_d^{\mathcal{F}}$	$k_{s,t}, k_{s,r}$	$d_{d,t}, d_{d,r}$
	(N)	(W)	(W)	(J)	(J)	(J)	(J)	(s)	(s)		[1/s]	(s)	[N/m], [Nm/rad]	[N·s/m], [Nm·s/rad]
Exp. 1	-10	0.03	0.01	0.1	0.1	1	1	2	2	$2\mathbf{I}_{6 \times 6}$	$2\mathbf{I}_{6 \times 6}$	$0.02\mathbf{I}_{6 \times 6}$	800, 25	300, 3
Exp. 2	-10	0.03	0.01	0.1	0.1	1	1	2	2	$2\mathbf{I}_{6 \times 6}$	$2\mathbf{I}_{6 \times 6}$	$0.02\mathbf{I}_{6 \times 6}$	800, 25	300, 3
Exp. 3	-3	0.05	0.01	0.1	0.1	2	1	2	2	$2\mathbf{I}_{6 \times 6}$	$2\mathbf{I}_{6 \times 6}$	$0.01\mathbf{I}_{6 \times 6}$	1500, 25	300, 3
Exp. 4	-3	0.05	0.01	0.1	0.1	2	1	2	2	$2\mathbf{I}_{6 \times 6}$	$2\mathbf{I}_{6 \times 6}$	$0.01\mathbf{I}_{6 \times 6}$	1500, 25	300, 3



(a) Interactive table-wiping task within U-Space.



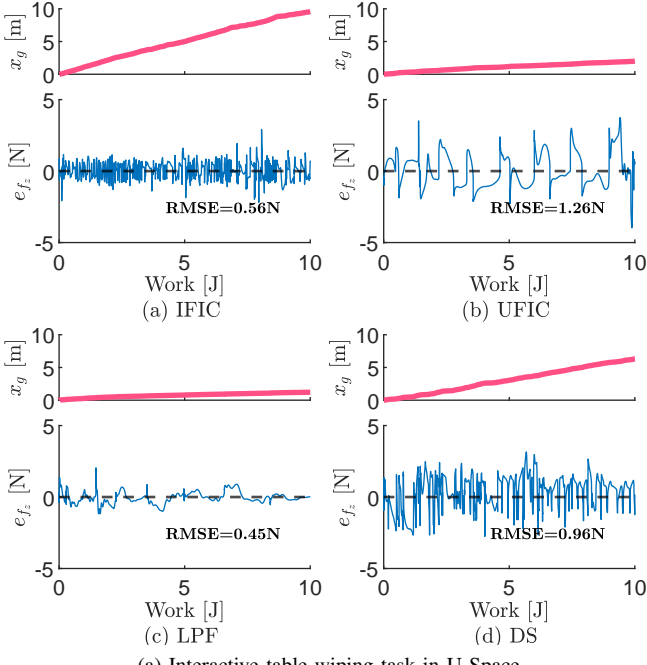
(b) Interactive table-wiping task within C-Space.

Fig. 3: Evaluation of IFIC in an interactive table-wiping task

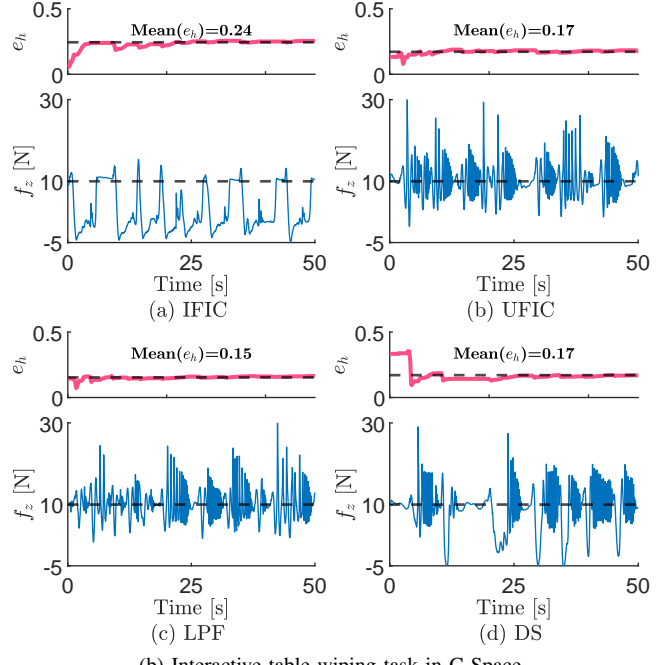
The performance of U-Space interaction with IFIC in the table-wiping task is illustrated in Fig. 3a. In the initial stage ($t < 50$ s), the operator applied sudden collisions along the impedance control direction. The energy in the interactive tank ${}^T\mathcal{E}_i$ decreased immediately, while the tank damping term $d_i = d_i, \tau d_{i,\mathcal{I}}$ increased due to the positive interaction power P_u , making the robot compliant under external interaction. The robot gradually resumed impedance control within $t_{l,i} = 2$ s following the interaction. During the remaining stages ($50 \leq t \leq 150$ s), the operator maintained continuous guidance along the U-Space. Throughout the interaction, the desired force was accurately tracked with a root mean square error (RMSE) of 0.81 N. C-Space interaction results for the table-wiping task are shown in Fig. 3b. When intended or unintended interactions drove the robot leave the workspace, the force controller was immediately detached due to positive P_c . Once the operator ceased guidance, the tank energy ${}^T\mathcal{E}_f$ gradually increased, and the damping $d_f = d_f, \tau d_{f,\mathcal{I}}$ decreased, allowing the force controller to resume operation. The negligible impact

force along the z -axis demonstrates that IFIC ensures safe interaction.

In the second experiment (Fig. 4a), the operator continuously interacted with the robot along the impedance control direction to compare the IE and z -axis force error e_{f_z} of the four methods. The IE e_h was defined as ratio of the distance traveled by the robot to the human work (integral of P_u for $P_u > 0$), i.e., $e_h = x_g/W_h$. For consistency, in all methods, the operator guided the robot back and forth along the y -axis. The guidance was paused at a marker position located 0.15 m away from the midpoint of the reciprocating motion, then the robot resumed impedance motion before the operator guided it in the opposite direction. This procedure was repeated until the total human work reached 10 J for each method. IFIC method achieved the highest mean IE of 1.02. As shown in Fig. 4b, IE and impact forces were further evaluated along the force control direction. The operator moved the robot upward along the z -axis to a specified height of 0.1 m and then released it in four methods. IFIC consistently exhibited minimal impact forces, whereas other methods caused violent impacts and bouncing against the



(a) Interactive table-wiping task in U-Space



(b) Interactive table-wiping task in C-Space

Fig. 4: Comparison of IFIC, UFIC, LPF, and DS for interactive table-wiping task: evaluation of force and efficiency.

table.

In the third experiment (Fig. 5), the four methods were compared during interactive ultrasound scanning on a soft-tissue phantom. The operator applied perturbations to the robot body to drive it away from the phantom. Force along the z -direction and P_c were recorded. Only IFIC prevented collisions with the phantom under these disturbances, while the other methods led to instability and robot bouncing.

In the fourth experiment (Fig. 6), interactive ultrasound scanning was performed on a human arm. During tidal probe scanning, sudden upward movements of the arm caused the probe to detach momentarily. IFIC responded safely to such disturbances, whereas other methods caused the robot to jump dangerously. In UFIC, contact force and velocity occasionally exceeded the KUKA Med safety limits, triggering a safety stop.

In summary, When the robot is forced or disturbed to leave the contact, or rebounds after recontact, the interaction may produce positive contact energy that tends to break passivity. To address this, the proposed IFIC attaches power-valve-controlled energy tanks to the interactive ports, which absorb the non-passive interaction energy while temporarily detaching the force controller to prevent contact-loss-induced instability. As a result, IFIC maintains stable and passive behavior and outperforms the other methods in response to external disturbances. In our experiments, a minimal energy budget of 0.8 J was assigned to the UFIC tanks. The UFIC force energy tank was never depleted during contact loss, allowing the controllers to remain active. Notably, during ultrasound scanning, rebound after contact with the arm or phantom increased the force tank energy of UFIC

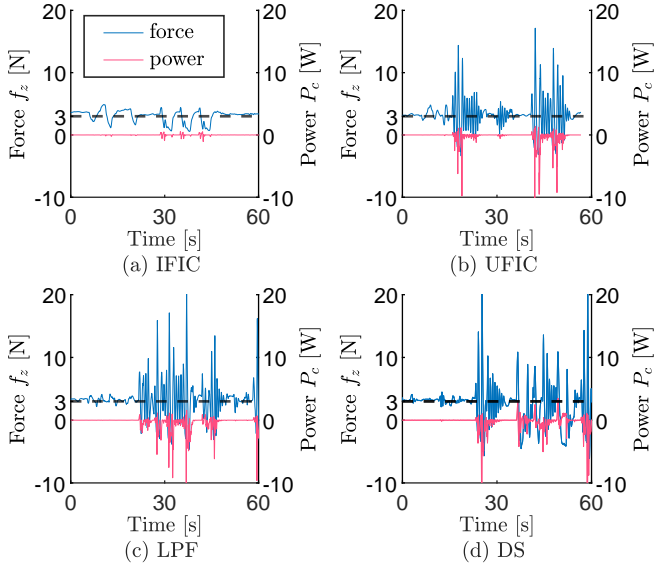


Fig. 5: Comparison of IFIC, UFIC, LPF, and DS in an interactive ultrasound scanning task on a soft-tissue phantom.

via negative force control power $\dot{x}^T F_f$. LPF performance was limited by noisy force signals, reducing sensitivity to human guidance. In U-Space, the impedance controller was deactivated only when the filtered force exceeded the 5 N force threshold to suppress friction noise. In C-Space, once the operator reduces or releases contact, the force controller reactivates, causing the robot to rapidly accelerate along the force control direction. And nominal DS method required accumulation of interaction energy before switching from

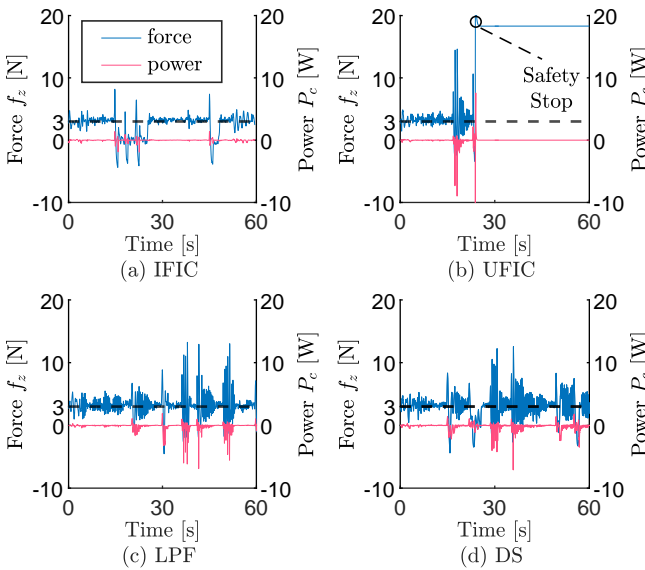


Fig. 6: Comparison of IFIC, UFIC, LPF, and DS in an interactive ultrasound scanning task on human arm.

precise tracking to compliant behavior, making them less responsive to instantaneous non-passive interactions.

VI. CONCLUSIONS

This paper addressed interaction safety and efficiency in force-impedance control. Future work will focus on a hierarchical framework, where IFIC serves as the low-level controller to ensure passivity, while a high-level layer estimates user intention in complex multitasking scenarios to adapt power flow and energy budget.

ACKNOWLEDGMENT

REFERENCES

- [1] M. Geravand, F. Flacco, and A. De Luca, "Human-robot physical interaction and collaboration using an industrial robot with a closed control architecture," in *2013 IEEE international conference on robotics and Automation*. IEEE, 2013, pp. 4000–4007.
- [2] V. Duchaine, B. M. St-Onge, D. Gao, and C. Gosselin, "Stable and intuitive control of an intelligent assist device," *IEEE transactions on haptics*, vol. 5, no. 2, pp. 148–159, 2012.
- [3] C. Wang and J. Zhao, "Role dynamic assignment of human–robot collaboration based on target prediction and fuzzy inference," *IEEE Transactions on Industrial Informatics*, vol. 20, no. 1, pp. 471–481, 2023.
- [4] M. Khoramshahi and A. Billard, "A dynamical system approach for detection and reaction to human guidance in physical human–robot interaction," *Autonomous Robots*, vol. 44, no. 8, pp. 1411–1429, 2020.
- [5] A. Kouris, F. Dimeas, and N. Aspragathos, "A frequency domain approach for contact type distinction in human–robot collaboration," *IEEE robotics and automation letters*, vol. 3, no. 2, pp. 720–727, 2018.
- [6] C. T. Landi, F. Ferraguti, L. Sabattini, C. Secchi, and C. Fantuzzi, "Admittance control parameter adaptation for physical human–robot interaction," in *2017 IEEE international conference on robotics and automation (ICRA)*. IEEE, 2017, pp. 2911–2916.
- [7] M. Ma and L. Cheng, "A human–robot collaboration controller utilizing confidence for disagreement adjustment," *IEEE Transactions on Robotics*, 2024.
- [8] M. Iskandar, A. Albu-Schäffer, and A. Dietrich, "Intrinsic sense of touch for intuitive physical human–robot interaction," *Science Robotics*, vol. 9, no. 93, p. eadn4008, 2024.
- [9] C. Y. Wong, L. Vergez, and W. Suleiman, "Vision-and tactile-based continuous multimodal intention and attention recognition for safer physical human–robot interaction," *IEEE Transactions on Automation Science and Engineering*, vol. 21, no. 3, pp. 3205–3215, 2023.
- [10] M. Angerer, S. Musić, and S. Hirche, "Port-hamiltonian based control for human–robot team interaction," in *2017 IEEE International Conference on Robotics and Automation (ICRA)*. IEEE, 2017, pp. 2292–2299.
- [11] G. Raiola, C. A. Cardenas, T. S. Tadele, T. De Vries, and S. Stramigoli, "Development of a safety-and energy-aware impedance controller for collaborative robots," *IEEE Robotics and automation letters*, vol. 3, no. 2, pp. 1237–1244, 2018.
- [12] C. T. Landi, F. Ferraguti, C. Fantuzzi, and C. Secchi, "A passivity-based strategy for coaching in human–robot interaction," in *2018 IEEE International Conference on Robotics and Automation (ICRA)*. IEEE, 2018, pp. 3279–3284.
- [13] F. Ferraguti, N. Preda, A. Manurung, M. Bonfe, O. Lambercy, R. Gassert, R. Muradore, P. Fiorini, and C. Secchi, "An energy tank-based interactive control architecture for autonomous and teleoperated robotic surgery," *IEEE Transactions on Robotics*, vol. 31, no. 5, pp. 1073–1088, 2015.
- [14] X. Ke, Y. Yu, K. Li, T. Wang, B. Zhong, Z. Wang, L. Kong, J. Guo, L. Huang, M. Idir *et al.*, "Review on robot-assisted polishing: Status and future trends," *Robotics and Computer-integrated manufacturing*, vol. 80, p. 102482, 2023.
- [15] Q. Wang, W. Wang, L. Zheng, and C. Yun, "Force control-based vibration suppression in robotic grinding of large thin-wall shells," *Robotics and Computer-Integrated Manufacturing*, vol. 67, p. 102031, 2021.
- [16] C. Schindlbeck and S. Haddadin, "Unified passivity-based cartesian force/impedance control for rigid and flexible joint robots via task-energy tanks," in *2015 IEEE international conference on robotics and automation (ICRA)*. IEEE, 2015, pp. 440–447.
- [17] S. Haddadin and E. Shahriari, "Unified force-impedance control," *The International Journal of Robotics Research*, vol. 43, no. 13, pp. 2112–2141, 2024.
- [18] M. Iskandar, C. Ott, A. Albu-Schäffer, B. Siciliano, and A. Dietrich, "Hybrid force-impedance control for fast end-effector motions," *IEEE Robotics and Automation Letters*, vol. 8, no. 7, pp. 3931–3938, 2023.
- [19] L. Peternel, N. Tsagarakis, and A. Ajoudani, "Towards multimodal intention interfaces for human–robot co-manipulation," in *2016 IEEE/RSJ international conference on intelligent robots and systems (IROS)*. IEEE, 2016, pp. 2663–2669.
- [20] S. Armleder, E. Dean-Leon, F. Bergner, and G. Cheng, "Interactive force control based on multimodal robot skin for physical human–robot collaboration," *Advanced Intelligent Systems*, vol. 4, no. 2, p. 2100047, 2022.
- [21] R. Ortega and M. W. Spong, "Adaptive motion control of rigid robots: A tutorial," *Automatica*, vol. 25, no. 6, pp. 877–888, 1989.
- [22] M. Suomalainen, Y. Karayannidis, and V. Kyriki, "A survey of robot manipulation in contact," *Robotics and Autonomous Systems*, vol. 156, p. 104224, 2022.
- [23] O. Khatib, "Inertial properties in robotic manipulation: An object-level framework," *The international journal of robotics research*, vol. 14, no. 1, pp. 19–36, 1995.
- [24] F. Ferraguti, C. Secchi, and C. Fantuzzi, "A tank-based approach to impedance control with variable stiffness," in *2013 IEEE international conference on robotics and automation*. IEEE, 2013, pp. 4948–4953.
- [25] E. Shahriari, L. Johannsmeier, E. Jensen, and S. Haddadin, "Power flow regulation, adaptation, and learning for intrinsically robust virtual energy tanks," *IEEE Robotics and Automation Letters*, vol. 5, no. 1, pp. 211–218, 2019.
- [26] Y. Michel, C. Ott, and D. Lee, "Safety-aware hierarchical passivity-based variable compliance control for redundant manipulators," *IEEE Transactions on Robotics*, vol. 38, no. 6, pp. 3899–3916, 2022.
- [27] M. Khoramshahi and A. Billard, "A dynamical system approach to task-adaptation in physical human–robot interaction," *Autonomous Robots*, vol. 43, no. 4, pp. 927–946, 2019.